Mechanics of Irradiation-Induced Structural Changes in a Lipid Vesicle

Xinyu Liao
Graduate Group in Applied Mathematics and Computational Science,
University of Pennsylvania,
Philadelphia, PA 19104
e-mail: xinyul@sas.upenn.edu

Prashant K. Purohit[1]
Graduate Group in Applied Mathematics and Computational Science,
University of Pennsylvania,
Philadelphia, PA 19104;
Department of Mechanical Engineering and Applied Mechanics,
University of Pennsylvania,
Philadelphia, PA 19104
e-mail: purohit@seas.upenn.edu

Irradiation-induced oxidation of lipid membranes is implicated in diseases and has been harnessed in medical treatments. Irradiation induces the formation of oxidative free radicals, which attack double bonds in the hydrocarbon chains of lipids. Studies of the kinetics of this reaction suggest that the result of the first stage of oxidation is a structural change in the lipid that causes an increase in the area per molecule in a vesicle. Since area changes are directly connected to membrane tension, irradiation-induced oxidation affects the mechanical behavior of a vesicle. Here, we analyze shape changes of axisymmetric vesicles that are under simultaneous influence of adhesion, micropipette aspiration, and irradiation. We study both the equilibrium and kinetics of shape changes and compare our results with experiments. The tension–area relation of a membrane, which is derived by accounting for thermal fluctuations, and the time variation of the mechanical properties due to oxidation play important roles in our analysis. Our model is an example of the coupling of mechanics and chemistry, which is ubiquitous in biology.
[DOI: 10.1115/1.4042429]

Keywords: oxidation, lipid membrane, adhesion

1 Introduction

Oxidative damage to lipids in cell membranes is increasingly being implicated as a cause of cell death, diseases, and aging since at least the early 1990s [1,2]. Controlled oxidative damage has also been used in treatment of certain diseases by a procedure called photodynamic therapy. The treatment induces oxidative damage in diseased cells through the use of photosensitizer, light, and oxygen in a proper combination [3,4]. The targets for oxidation are poly-unsaturated lipids, or lipids with double-bonds in their hydrocarbon chains [3–5]. Even though in experiments and in photodynamic therapy reactive oxygen is produced using photosensitive molecules, these are also generated enzymatically and through respiration [1] during normal life processes. As such, much is known about the chemical changes to the lipid molecules due to oxidation [1,5,6], but little attention has been paid to the mechanics of lipid membranes subjected to irradiation-induced oxidation. In particular, irradiation results in time-varying mechanical properties of vesicles [7], yet there are no models that account for this variation in vesicle mechanics.

Oxidative damage to lipids is known to proceed in two major steps [4]. In the first step, oxidation of double bonds causes an increase in the area per molecule of the lipid membrane by about 15–20% [5]. This is accompanied by a decrease of area expansion modulus K_A and an increase in thermal undulations [7]. In the second step (whose effects are prominent if irradiation continues for long periods), scission of the hydrocarbon chain may occur and vesicle shrinkage occurs due to formation of pores [4]. The kinetics of both these oxidation steps can be described as first-order reactions [6] and the rate constants appearing in them have been fitted to experimental data [4]. However, the mechanics of a vesicle under simultaneous action of forces and irradiation remains to be investigated even though it plays an important role in cell membrane functions [8]. For example, membrane tension is known to regulate exo- and endo-cytosis, actin network assembly, and motility in live cells [9] and may also contribute to cell growth [10]. Therefore, it is conceivable that changes in membrane tension caused by irradiation-induced area increases could affect cellular processes.

In this paper, we will build on previous experimental studies and develop a model to analyze vesicle shapes and mechanics under the action of forces and irradiation. Since adhesion and micropipette aspiration are routinely used in experimental measurements, we will focus on vesicle shapes in these assays. We will analyze both equilibrium and kinetics of irradiation-induced shape changes and take account of thermal fluctuations, which contribute significantly to membrane biophysical behavior [11]. We will constrain our analysis to the first step of oxidation, which involves structural changes that increase area and decrease elastic moduli, and to axisymmetric vesicles since these are analytically tractable [12–14]. The mechanics in the second step of oxidation is more challenging and is not treated here since it involves lipid hydrocarbon chain scission and pore formation, which are amenable to molecular simulation. Our model connects vesicle shape, mechanics, and kinetics of irradiation-induced structural changes within a tractable analytical framework that can be used to interpret experiments and generate falsifiable predictions. We are not aware of any other models that accomplish this even though there are detailed analyses of the kinetics of lipid oxidation [4,15], and a multitude of papers that predict vesicle shape changes in response to applied forces or other mechanical constraints [16–18]. In the following, we consider (a) equilibrium shapes of vesicles under the action of forces and irradiation-induced structural change in Sec. 2, and (b) the kinetics of shape evolution due to loading and irradiation-induced structural change in Secs. 3 and 4. We give a brief conclusion in Sec. 5.

2 Equilibrium Shapes of Adhered Vesicles Under Irradiation

2.1 Review of Equations to Compute Shapes of Adhered Vesicles Under Applied Force. To see how area changes due to irradiation enter into the computation of vesicle shape and mechanics, we must first review the mechanics of adhered vesicles. Consider a vesicle that is originally spherical with radius

[1]Corresponding author.

Contributed by the Applied Mechanics Division of ASME for publication in the Journal of Applied Mechanics. Manuscript received October 15, 2018; final manuscript received December 23, 2018; published online January 30, 2019. Assoc. Editor: Pedro Reis.

R_0. The vesicle is surrounded by fluid (usually water for lipid vesicles) that may contain osmolytes to control its volume [16]. When it adheres to a surface, it remains axisymmetric but might not be spherical. Hence, the three-dimensional shape of the vesicle can be described by a closed curve in two dimensions with an axis of rotational symmetry [19]. Then, the pressure difference p is related to the tension τ and local mean curvature through the Young–Laplace law

$$p = 2\tau H = \tau(\kappa_1 + \kappa_2) \tag{1}$$

where κ_1 is the meridional principal curvature, κ_2 is the principal curvature along lines perpendicular to the meridians, and $H = \kappa_1 + \kappa_2/2$ is the mean curvature. In experiments, the deformation of the vesicle happens in such a way as the volume remains fixed (due to osmotic constraints), so the pressure difference p must change and we will determine it using the Young–Laplace law given earlier.

Adhesion changes the tension in the membrane and also causes an increase in the area by 1–2% [20,21]. However, this area change is not taken into account in most analyses of adhering vesicles [13,17,19]. Typically, in experiments, the tension is in the region where the fluctuations of the vesicle get pulled out to cause the increase in area. Let A be the area of the membrane in the absence of fluctuations and tension. Let $A_{\text{red}}(\tau)$ represent the amount by which the projected area is reduced below the area A by thermal fluctuations at tension τ and temperature T, then we know that [19,22]

$$\frac{A_{\text{red}}(0) - A_{\text{red}}(\tau)}{A} = \frac{k_B T}{8\pi K_b}\log\left(1 + \frac{\tau A}{\pi^2 K_b}\right) + \frac{\tau}{K_A} \tag{2}$$

where k_B is the Boltzmann constant, K_b is the bending modulus of the membrane, and K_A is the stretching or area expansion modulus.

Now, let us assume that the vesicle is adhered to a substrate and a force F is exerted on it by a micropipette while it remains axisymmetric. $F > 0$ when the force is pushing the vesicle against the substrate. If we make a cut perpendicular to the axis of the vesicle where the radius is $r(s)$ and the tangent angle to the contour of the axisymmetric shape is $\phi(s)$, s being a position parameter along the arc length of the closed curve, then equilibrium demands that

$$2\pi\tau r(s)\sin\phi(s) = \pi r^2(s)p - F \tag{3}$$

The vesicle makes contact with the substrate over a circular region of radius r_1. The angle ϕ_1 at $r = r_1$ depends on the adhesion energy per unit area between the vesicle and the substrate. If Γ is the adhesion energy per unit area, then

$$\Gamma = \tau(1 - \cos\phi_1) \tag{4}$$

which is known as the Young–Dupre equilibrium [17]. To get the vesicle shape, we note that

$$\frac{dr}{ds} = \cos\phi(s) = \sqrt{1 - \sin^2\phi(s)}, \quad \frac{dz}{ds} = \sin\phi(s) \tag{5}$$

where $\sin\phi(s)$ is given by Eq. (3) in terms of $r(s)$ and F, and $z(s)$ is the height of point s with $z(0) = 0$ at the equator of the vesicle. We can therefore integrate the differential equation for $r(s)$ and get

$$r(s) = \frac{\sqrt{2}\tau}{p}\sqrt{1 + \frac{Fp}{2\pi\tau^2} + \sqrt{1 + \frac{Fp}{\pi\tau^2}}\cos\frac{ps}{\tau}} \tag{6}$$

Now, we claim that the term $\kappa_1 + \kappa_2$ in Eq. (1) is a constant. As pointed out in standard texts in differential geometry [23], the mean curvature $\kappa_1 + \kappa_2/2$ equals a constant c_0 for an axisymmetric shape if and only if

$$\frac{d\left(r\frac{dz}{ds}\right)}{ds} = c_0\frac{d(r^2)}{ds} \tag{7}$$

By using Eqs. (3) and (5), it is easy to show that Eq. (7) is equivalent to

$$\frac{p}{2\tau} = c_0 \tag{8}$$

which implies that $\kappa_1 + \kappa_2 = p/\tau$. Therefore, the Young–Laplace law Eq. (1) is automatically satisfied on the nonadhered part of the vesicle. Let $s = s_1$ be such that $r(s_1) = r_1$ and $\phi(s_1) = \phi_1$ at the bottom of the vesicle where adhesion occurs. Then the expression for s_1 becomes

$$\cos\frac{ps_1}{\tau} = \frac{\frac{p^2r_1^2}{2\tau^2} - 1 - \frac{Fp}{2\pi\tau^2}}{\sqrt{1 + \frac{Fp}{\pi\tau^2}}} \tag{9}$$

From Eq. (9), we get

$$s_1 = -\frac{\tau}{p}\cos^{-1}\left(\frac{\frac{p^2r_1^2}{2\tau^2} - 1 - \frac{Fp}{2\pi\tau^2}}{\sqrt{1 + \frac{Fp}{\pi\tau^2}}}\right) \tag{10}$$

We must solve for $\sin\phi_1$ using the Young–Dupre equilibrium Eq. (4)

$$\sin\phi_1 = \sqrt{1 - \left(1 - \frac{\Gamma}{\tau}\right)^2} = \frac{pr_1}{2\tau} - \frac{F}{2\pi r_1\tau} \tag{11}$$

By using Eq. (11), r_1 can be solved

$$r_1 = \frac{\tau}{p}\left(\sin\phi_1 + \sqrt{\sin^2\phi_1 + \frac{Fp}{\pi\tau^2}}\right) \tag{12}$$

At the top of the vesicle, $r = r_2$. If $s = s_2$ at the top of the vesicle, then it can be determined using

$$s_2 = \frac{\tau}{p}\cos^{-1}\left(\frac{\frac{p^2r_2^2}{2\tau^2} - 1 - \frac{Fp}{2\pi\tau^2}}{\sqrt{1 + \frac{Fp}{\pi\tau^2}}}\right) \tag{13}$$

It should be noted that $1 + (Fp/2\pi\tau^2) > \sqrt{1 + (Fp/\pi\tau^2)}$, which implies that $r_2 \neq 0$ if $F \neq 0$. Integrating Eq. (5) for $z(s)$, we get

$$z(s) = \int_0^s \sin\phi(s)\,ds = \int_0^s\left(\frac{pr(s)}{2\tau} - \frac{F}{2\pi\tau r(s)}\right)ds \tag{14}$$

where $r(s)$ is given by Eq. (6). We substitute for $r(s)$ to get

$$z(s) = \frac{1}{\sqrt{2}}\int_0^s\sqrt{1 + \frac{Fp}{2\pi\tau^2} + \sqrt{1 + \frac{Fp}{\pi\tau^2}} - 2\sqrt{1 + \frac{Fp}{\pi\tau^2}}\sin^2\frac{ps}{2\tau}}\,ds - \frac{Fp}{2\sqrt{2}\pi\tau^2}\int_0^s\frac{ds}{\sqrt{1 + \frac{Fp}{2\pi\tau^2} + \sqrt{1 + \frac{Fp}{\pi\tau^2}} - 2\sqrt{1 + \frac{Fp}{\pi\tau^2}}\sin^2\frac{ps}{2\tau}}} \tag{15}$$

This can be reduced to

$$z(s) = \frac{\tau}{p}\left(1 + \sqrt{1 + \frac{Fp}{\pi\tau^2}}\right)\int_0^{\frac{ps}{2\tau}} \sqrt{1 - m^2\sin^2\theta}\, d\theta - \frac{F}{\pi\tau}\frac{1}{1 + \sqrt{1 + \frac{Fp}{\pi\tau^2}}}\int_0^{\frac{ps}{2\tau}} \frac{d\theta}{\sqrt{1 - m^2\sin^2\theta}} \tag{16}$$

where

$$m^2 = \frac{2\sqrt{1 + \frac{Fp}{\pi\tau^2}}}{1 + \frac{Fp}{2\pi\tau^2} + \sqrt{1 + \frac{Fp}{\pi\tau^2}}} \leq 1 \tag{17}$$

Recognizing the incomplete elliptic integrals above, we write

$$z(s) = \frac{\tau}{p}\left(1 + \sqrt{1 + \frac{Fp}{\pi\tau^2}}\right)E\left(\frac{ps}{2\tau}|m\right) - \frac{F}{\pi\tau}\frac{1}{1 + \sqrt{1 + \frac{Fp}{\pi\tau^2}}}F\left(\frac{ps}{2\tau}|m\right) \tag{18}$$

where $E((ps/2\tau)|m)$ is the incomplete elliptic integral of the second kind with modulus m and $F((ps/2\tau)|m)$ is the incomplete elliptic integral of the first kind with modulus m. We use Eqs. (6) and (18) to plot vesicle shapes later in this paper.

When $F = 0$, from Eqs. (12) and (9), we see that

$$r_1 = \frac{2\tau}{p}\sqrt{\frac{2\Gamma}{\tau} - \frac{\Gamma^2}{\tau^2}} \tag{19}$$

$$\cos\frac{ps_1}{\tau} = 2\left(\frac{2\Gamma}{\tau} - \frac{\Gamma^2}{\tau^2}\right) - 1 \tag{20}$$

Hence, the shape of the adhered vesicle is described by

$$r(s) = \frac{2\tau}{p}\cos\frac{ps}{2\tau} \tag{21}$$

$$z(s) = \frac{2\tau}{p}\sin\frac{ps}{2\tau} \tag{22}$$

$$s_1 = -\mathrm{sgn}(\cos\phi_1)\frac{\tau}{p}\cos^{-1}\left(\frac{4\Gamma}{\tau} - \frac{2\Gamma^2}{\tau^2} - 1\right) \tag{23}$$

$$s_2 = \frac{\tau}{p}\cos^{-1}\left(\frac{p^2 r_2^2}{2\tau^2} - 1\right) \tag{24}$$

Now, let us consider the case of a spherical vesicle of radius R_0 about to adhere to a substrate. The vesicle is a spherical section of radius R after adhesion and its shape is given by Eqs. (21)–(24). Then the volume is easily computed

$$V = \frac{1}{2}\pi\left(\sqrt{R^2 - r_2^2} + \cos\phi_1 R\right)\cdot\left(R^2\sin^2\phi_1 + r_2^2 + \frac{1}{3}\left(\sqrt{R^2 - r_2^2} + \cos\phi_1 R\right)^2\right) \tag{25}$$

where $R = 2\tau/p$ is derived from the Young–Laplace law Eq. (1). Similarly, the surface area of the spherical section can be computed

$$A_{\mathrm{sp}} = 2\pi R\left(\sqrt{R^2 - r_2^2} + \cos\phi_1 R\right) \tag{26}$$

The area of the circular portion in contact with the substrate is $\pi R^2\sin^2\phi_1$. Let A_0 be the contour area when the vesicle is a perfect sphere. Then we have $A_0 = A_{\mathrm{red}}(0) + 4\pi R_0^2$. If the changes in area are due to stretching out of thermal fluctuations, then $A_{\mathrm{red}}(0) = A_0(k_BT/8\pi K_b)\log(A_0/b^2)$ [19]. Hence, we can compute A_0 through

$$4\pi R_0^2 = A_0\left(1 - \frac{k_BT}{8\pi K_b}\log\frac{A_0}{b^2}\right) \tag{27}$$

where $b = 1$ nm is intermolecular spacing [19].

2.2 Application to an Adhered Vesicle. We will now use the ideas above to estimate the adhesion energy per unit area, Γ, from experimental data. In an experiment conducted by Aoki et al. [24], the radius of a dipalmitoylphosphatidylcholine giant unilamellar vesicle after adhesion is estimated to be $R = 1.73\times10^{-5}$ m (using the scale bar in Fig. 1(*c*) of Ref. [24]). We will take stretching modulus $K_A = 230\,\mathrm{mN\cdot m^{-1}}$ and bending modulus $K_b = 21k_BT = 21\times4.1$ pN·nm at $T = 300$ K as typical values for dipalmitoylphosphatidylcholine vesicles [7,19]. Then, A_0 can be numerically solved from Eq. (27). We assume there is no thermal fluctuation in the part of the vesicle attached to the substrate. Let A^t denote the contour area of the fluctuating part of the vesicle (A^t would be the area at $T = 0$), then we have $A^t = A_0 - \pi R^2\sin^2\phi_1 - \pi r_2^2$. Under tension τ, A_{red} (τ) can be computed through

$$A_{\mathrm{red}}(\tau) = A^t - 2\pi R(\sqrt{R^2 - r_2^2} + \cos\phi_1 R) \tag{28}$$

At present, ϕ_1, R_0, and τ are all unknown. They will be determined by the Young–Dupre equilibrium Eq. (4), tension area relation, and volume constraints, respectively, through

$$\frac{A^t\frac{k_BT}{8\pi K_b}\log\frac{A^t}{b^2} - A^t + 2\pi R\left(\sqrt{R^2 - r_2^2} + \cos\phi_1 R\right)}{A^t} = \frac{k_BT}{8\pi K_b}\log\left(1 + \frac{\tau A^t}{\pi^2 K_b}\right) + \frac{\tau}{K_A} \tag{29}$$

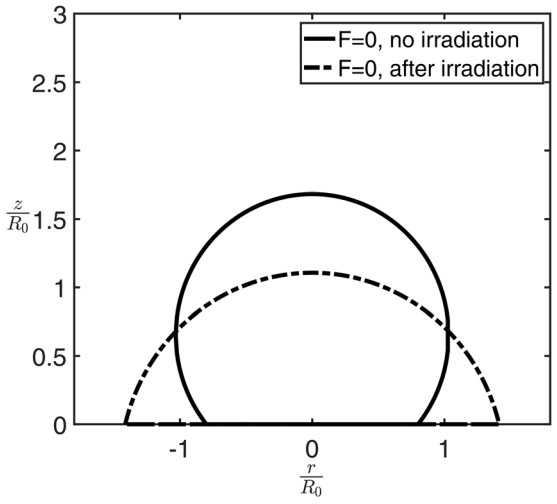

Fig. 1 Computed vesicle shapes before (solid line) and after (dashed line) irradiation for parameters in Aoki et al. [24]. These shapes are in qualitative agreement with shapes in Ref. [24] validating our model.

$$\frac{4}{3}\pi R_0^3 = \frac{1}{2}\pi\left(\sqrt{R^2 - r_2^2} + \cos\phi_1 R\right) \cdot \left(R^2\sin^2\phi_1 + r_2^2 + \frac{1}{3}\left(\sqrt{R^2 - r_2^2} + \cos\phi_1 R\right)^2\right) \quad (30)$$

Here, we take $r_2 = 0$ since there is no pipette or adhering surface on the top of the vesicle. Now, Eqs. (29), (30), and (4) are three equations for three unknowns R_0, τ, and ϕ_1 if the adhesion energy per unit area Γ is given. However, Γ is not immediately known from the experiments of Aoki et al. [24] who report that r_1/R_0 lies between 0.5 and 0.7 when there is no irradiation. Using this information, R_0, τ, and ϕ_1 can be numerically computed by choosing r_1/R_0 to be in this range and combining with Eqs. (29) and (30). Then, Γ is estimated from Eq. (4). We find that Γ is between 10^{-10} N/m and 10^{-7} N/m. Other experimental and theoretical works [20,25] estimate that Γ mostly lies between 10^{-5} N/m and 10^{-2} N/m. Trial and error reveals that the estimated Γ is quite sensitive to changes in r_1/R_0. To make progress, we take $\Gamma = 2.53 \times 10^{-5}$ N/m, which corresponds to $r_1/R_0 \approx 0.8$ for experiments in Ref. [24]. The uncertainty in Γ is probably also the reason why Sankhagowit et al. [4] measure changes in area using optical traps rather than adhesion.

2.3 Shapes of Adhered Vesicles Before and After Irradiation With Zero Force. Once the three unknowns R_0, τ, and ϕ_1 have been solved, we can plot the shape of an adhered vesicle using Eqs. (21)–(24). Next, we must account for increases in vesicle surface area caused by irradiation. Let A be the area after irradiation, which can be represented as

$$A = A_0 \times \alpha \quad (\alpha > 1) \quad (31)$$

In Ref. [24], the maximum surface area ratio is $\alpha = 1.1801$, 1.1878, 1.1936 under irradiation powers 1/4, 1/32, 1, respectively. Here, 1 represents maximum radiation intensity and we refer the reader to Aoki et al. [24] for quantitative details. We take $\alpha = 1.1878$ in Eq. (31) as an example. We are not aware of measurements of K_b as a vesicle suffers oxidation. However, Boal and Boal [19] point out that K_b is proportional to K_A, or $K_b = \zeta K_A$ where ζ is a constant depending on the bilayer thickness. The bilayer thickness is determined by the length of the hydro-carbon chains in the lipid tails, which does not change in the first step of oxidation before chain scission happens. Hence, from the known values of K_A after irradiation is completed, we can estimate the K_b of oxidized vesicles. Using $K_A = 80\,\mathrm{mN\cdot m^{-1}}$ [7] after irradiation for DOPC, the corresponding $K_b = 7.3\ k_BT$. Note that A_0 is dependent on K_b through Eq. (27); hence, it will change when K_b is changed. Then, with Γ known from Sec. 2, we can solve for the new values of R, ϕ_1, and τ in the adhered vesicle after irradiation. Accordingly, the adhered vesicle shapes before and after irradiation can be plotted using Eqs. (21)–(24). The shapes are shown in Fig. 1. In both situations (with and without irradiation), the shapes of the vesicle adhering to the substrate under no force in the experiments of Aoki et al. [24] are qualitatively described by our model.

2.4 Shapes of Adhered Vesicles Under Tensile and Compressive Forces After Irradiation. Tensile forces are exerted on adhered vesicles (with known mechanical properties) to estimate the adhesion energy density Γ on various substrates [13], while compressive forces are exerted on cells to estimate membrane tension [9]. The changes of vesicle (or cell) shape under these circumstances can be measured and used to estimate Γ, τ, etc. In a previous work, Lin and Freund [17] studied the shapes of an adhered vesicle under pulling force in the absence of irradiation. Our goal here is to determine how shapes change when both pulling force and irradiation are applied. Following the assumptions of Brochard-Wyart and deGennes [13], we consider a vesicle bound on one side to a pipette with fixed pipette radius $r_2 = 0.2\,R_0$ and constant contact angle $\phi_1 = \pi/4$. The height of the cylindrical portion of the vesicle in the pipette, h, is adjustable [26]. For convenience, we assume the top of the vesicle is flat and that there is no thermal fluctuation in the part of the vesicle inside the pipette and the part that is adhered. When $F \neq 0$, the constraint equations are only the tension–area relation and volume constraint. Since Γ is given and ϕ_1 is fixed, τ can easily be obtained from Eq. (4). Thus, Eqs. (29) and (30) are, respectively, replaced by

$$\frac{A_t\frac{k_BT}{8\pi K_b}\log\frac{A_t}{b^2} - \left(A_t - 2\pi\int_{s_1}^{s_2} r(s)ds\right)}{A_t} = \frac{k_BT}{8\pi K_b}\log\left(1 + \frac{\tau A_t}{\pi^2 K_b}\right) + \frac{\tau}{K_A} \quad (32)$$

$$\frac{4}{3}\pi R_0^3 - \pi r_2^2 h = \frac{\tau^3}{p^3}\pi\left(1 + \sqrt{1 + \frac{Fp}{\pi\tau^2}}\right)^3 \int_{\frac{ps_1}{2\tau}}^{\frac{ps_2}{2\tau}} \left(\sqrt{1 - m^2\sin^2\theta}\right)^3 d\theta - \frac{F\tau}{p^2}\left(1 + \sqrt{1 + \frac{Fp}{\pi\tau^2}}\right)\int_{\frac{ps_1}{2\tau}}^{\frac{ps_2}{2\tau}} \sqrt{1 - m^2\sin^2\theta}\,d\theta \quad (33)$$

where the area of the fluctuating part of the vesicle A_t in Eq. (32) is replaced by

$$A_t = A - (\pi r_1^2 + \pi r_2^2 + 2\pi r_2 h) \quad (34)$$

Recall that r_2 is the radius of the flat region of the vesicle inside the pipette. We have two equations, Eqs. (32) and (33), for two unknowns p and h, which can be solved numerically.

Once we solve for p and h, we can plot the shapes of the vesicle for both $F < 0$ (tensile force causing detachment) and $F > 0$ (compressive force causing adhesion). In Fig. 2(*b*), we plot the shapes when a tensile force F is applied. The corresponding contact radii are plotted in Fig. 2(*a*). Similarly, in Fig. 3, we plot the shapes and the corresponding contact radii when a compressive force F is applied. The predictions in these figures can be tested with routine micropipette experiments. For $F < 0$, there are three important points A_1, B_1, and C_1, where A_1 represents the start of the detachment process when the contact radius is maximum, B_1 represents the state of maximum achievable detachment force, which is $F_{cr} \approx 0.43\,pR_0^2$ compared to $F_{cr} \approx 0.30\,pR_0^2$ in the case without irradiation studied by Lin and Freund [17]. Since the nondimensional initial contact radius $r_1/R_0 \approx 0.7$ in our work is slightly larger than the one $r_1/R_0 \approx 0.6$ in Ref. [17], it requires stronger force to detach the vesicle from the substrate after

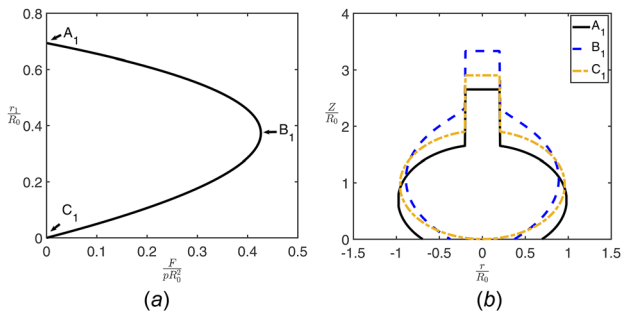

(*a*) (*b*)

Fig. 2 (*a*) Prediction of dependence of dimensionless contact radius r_1/R_0 on dimensionless pulling force F/pR_0^2 under irradiation. (*b*) Prediction of shapes during detachment. In (*b*), the height of the vesicle inside the pipette is not fully shown to focus on vesicle shapes. The heights inside the pipette at A_1, B_1, C_1 are, respectively, $h_{A_1}/R_0 = 3.73$, $h_{B_1}/R_0 = 3.65$, $h_{C_1}/R_0 = 3.89$. The nonmonotonic dependence of r_1 on F is similar to Lin and Freund [17].

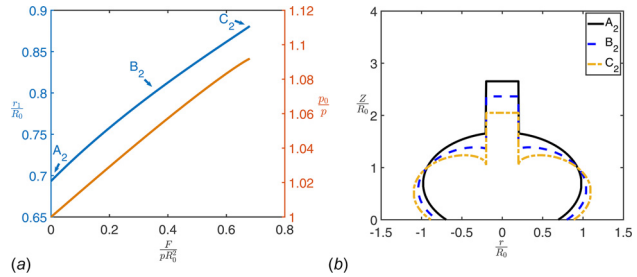

Fig. 3 (*a*) Prediction of dependence of dimensionless contact radius r_1/R_0 on dimensionless pushing force F/pR_0^2 and dependence of dimensionless pressure difference p/p_0 on F/pR_0^2 under irradiation where p_0 is the pressure difference in the absence of force. (*b*) Prediction of shapes during compression. In (*b*), the height of the vesicle in the pipette is not fully shown to focus on vesicle shapes. The heights inside the pipette at A_2, B_2, C_2 are, respectively, $h_{A_2}/R_0 = 3.73$, $h_{B_2}/R_0 = 3.49$, $h_{C_2}/R_0 = 2.96$.

irradiation that increases contact area. In addition, C_1 represents the state when detachment is about to occur. As pointed out by Lin and Freund [17], the vesicle is in stable equilibrium from A_1 to B_1 while from B_1 to C_1, it is not. As for $F > 0$, we found that the pressure difference and contact area monotonically increase as the compressive force increases, as expected.

3 Kinetics of Attachment of Vesicle Under Irradiation

So far, we have gained some understanding of how vesicle shapes and mechanics can be modulated by adhesion, applied forces, and irradiation. Our methods can be used to estimate difficult to measure quantities (i.e., pressure difference, adhesion energy, tension) when other experimental observables (i.e., contact radius, vesicle height sucked into pipette) are measured under various applied forces and irradiation intensities. Next, we hope to garner some insights into the kinetics of processes, such as adhesion and oxidation, that happen simultaneously in experiments.

3.1 Oxidation Kinetics and Corresponding Area Increase. In this section, we study a palmitoyloleoylphosphatidylcholine (POPC) vesicle with radius $R_0 = 0.75 \times 10^{-5}$ m under irradiation at constant intensity. In the experiment conducted by Weber et al. [7], the top of the vesicle is sucked into a micropipette with radius $r_2 = 0.47\ \mu$m and the constant membrane tension is fixed at $0.7\ \text{mN}\cdot\text{m}^{-1}$. Since there is no adhesion, the contact radius $r_1 = 0$.

Sankhagowit et al. [4] illustrated that oxidation has two stages where OX1 is an oxidized lipid which is the product of the first reaction and it occupies more membrane area than nonoxidized DOPC and OX2 is the product of the second reaction, which occupies less surface area than DOPC. For simplicity, we assume only OX1 appears during the irradiation and the model built for DOPC could be applied to POPC, since both have double bonds. Also, the bending modulus of POPC is about $20.7\ k_BT$ at room temperature $T = 303$ K [27] that is not too different from the bending modulus of DOPC. The second reaction, which involves OX2, is known to be slower than that involving OX1 and its effects (decrease in area) are seen when irradiation is continued for a long time [4]. We will confine our analysis to only the early stages of irradiation when area increases are seen. Sankhagowit et al. [4] gives the formula to compute the concentration of OX1

$$C_{\text{OX1}}(t) = 1 - e^{-k_1 t} \tag{35}$$

where k_1 scales roughly as $I^{1/2}$ where I is the radiation intensity or radiation power. Let A_{OX1} be the area per lipid of OX1 relative to that of POPC (i.e. $A_{\text{POPC}} = 1$, $A_{\text{OX1}} > 1$). Then the surface area increment $S(t)$ can be expressed as

$$\begin{aligned} S(t) &= A_{\text{POPC}}(1 - C_{\text{OX1}}) + A_{\text{OX1}}C_{\text{OX1}} - 1 \\ &= (A_{\text{OX1}} - 1)(1 - e^{-k_1 t}) \end{aligned} \tag{36}$$

When the irradiation time is sufficiently long, the surface area will reach $\max_{t\geq 0} S(t)$ and then not change. This requires that $A_{\text{OX1}} = \max_{t\geq 0} S(t) + 1$. In order to be consistent with the experimental data in Fig. 3(*a*) of Weber et al. [7], we need to set $A_{\text{OX1}} = 1.1388$, $k_1 = 0.1979\ \text{s}^{-1}$, as shown in Fig. 4(*a*) by the orange line (passing through the experimental data). Note that the value of k_1 used here is in the same range as that reported by Sankhagowit et al. [4]. The good fit of the orange curve to the experimental data from Ref. [7] shows that our assumption of confining attention to the first step of oxidation is justified. Now, Eqs. (32) and (33) can be used again to solve the two unknowns p, h. In order to do so, we need to (a) set $r_1 = 0$, $r_2 = 4.7\ \mu$m in Eq. (34), (b) in Eq. (31) the surface area should be a function of time $A(t) = A_0 \times (1 + S(t))$, where A_0 can be solved numerically from Eq. (27) based on vesicle initial radius $R_0 = 0.75 \times 10^{-5}$ m, (c) $S(t)$ is given in Eq. (36) and (d) the mechanical moduli K_A and K_b vary with time as discussed later.

Weber et al. [7] point out that the stretching modulus of vesicles, K_A, varies as irradiation progresses. Ordinarily, the mechanical properties of homogeneous vesicles are constants, but the appearance of an oxidized phase during irradiation decreases K_A. This oxidized phase appears everywhere on the vesicle since irradiation is applied globally; hence, K_A is taken to be independent of position. Since the fraction of the oxidized phase increases with time, the modulus K_A decreases with time. We use the information in Fig. 5 of Ref. [7] to treat K_A as a function of irradiation time t : $K_A = 230\ \text{mNm}^{-1} - 1.6\ \text{mNm}^{-1}\text{s}^{-1} \cdot t, 0 \leq t \leq 50$ s. Since K_b is proportional to K_A, the variation of K_b with time can be estimated if the initial $K_b = 20.7\ k_BT$ for the POPC vesicle before irradiation is known. Note that K_b plays an important role at low tensions, while K_A weighs in at high tension $\tau > 10^{-4}$ N/m. This can be understood from the fact that in the low tension regime, the log term dominates in Eq. (2) since $(\tau/K_A) \ll (k_BT/8\,\pi K_b)\log(1 + (\tau A_t/\pi^2 K_b))$, while at high tension, the thermal fluctuations are pulled out and the area increases linearly with tension as dictated by K_A. The result for the predicted pressure difference p/p_0 as irradiation progresses is shown in Fig. 4(*b*) and the result for the predicted pipette height h/h_0 is shown in Fig. 4(*a*). Note that the h/R_0 values for $\tau = 0.7\ \text{mN m}^{-1}$ are similar to the insets in Fig. 3(*a*) of Ref. [7] where h/R_0 is between 1 and 2 suggesting that our analysis is reasonable.

3.2 Ordinary Differential Equation Model of Contact Radius Increase Without Irradiation. Now, we study the dynamics of an initially spherical vesicle (with initial contact radius $r_1^{\text{init}} = 10$ nm and initial radius $R_0 = 1.68 \times 10^{-5}$ m consistent with the experiment in Ref. [24]) adhering to the substrate in

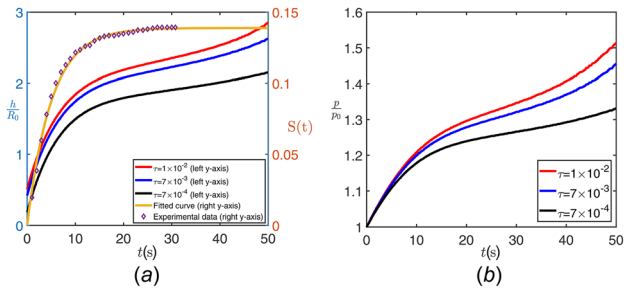

Fig. 4 (*a*) Prediction of dependence of dimensionless pipette height h/R_0 (left *y*-axis) on irradiation time *t*. The orange line is a fit of Eq. (36) to the experimental data of Weber et al. [7] for fractional change in vesicle area (right *y*-axis) as function of time. (*b*) Prediction of dependence of dimensionless pressure difference p/p_0 on irradiation time *t*. (See online for color version.)

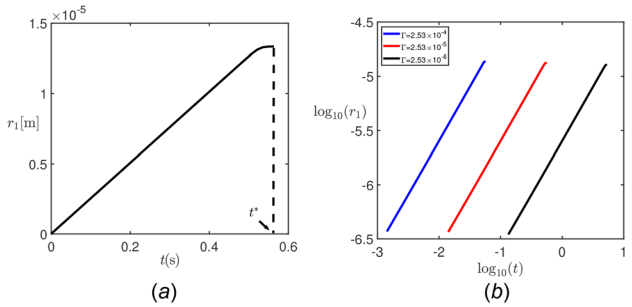

Fig. 5 (*a*) Prediction of time evolution of contact radius r_1 in the absence of irradiation. (*b*) Comparison between different Γ for the time of vesicle finishing adhesion on substrate in the absence of irradiation. See online for color version.

the absence of irradiation ($\alpha = 1$). In this context, we do not consider a pipette for aspiration on the top ($h = 0$, $r_2 = 0$, $F = 0$). Note that $S(t) = 0, \forall t \geq 0$ when there is no irradiation. As there is no applied force, the vesicle remains spherical in the unadhered region. Let $R(t)$ denote the radius of the spherical cap at time t. Then, $A^t(0) = A_0$, and $A^t(t) = A_0 \cdot (1 + S(t)) - \pi R^2(t) \sin^2\phi_1(t)$. From Ref. [20], we know that the tension τ is determined by

$$\tau = \frac{\pi^2 K_b}{a_0^2} \exp\left(-\frac{8\pi K_b}{k_B T}\epsilon\right) \tag{37}$$

where a_0^2 is the surface area of a lipid molecule with linear size $a_0 \approx 0.8\,\text{nm}$, and $\epsilon = (A^t(t) - 2\pi R^2(t)(1 + \cos\phi_1))/(2\pi R^2(t)(1 + \cos\phi_1))$ denotes the area strain of the membrane, which is the proportion of the surface area stored in the undulations. Note that Eq. (37) is very close to the inverse formula of Eq. (8.74) in Ref. [19], which is valid in the low tension regime. The constraint for fixed volume Eq. (32) at time t can be rewritten as

$$\frac{4}{3}\pi R_0^3 = \pi R(t)^3 \left(\frac{2}{3} + \cos\phi_1(t) - \frac{\cos^3\phi_1(t)}{3}\right) \tag{38}$$

Thus, $R(t)$ can be expressed as a function of contact angle $\phi_1(t)$

$$R(t) = \frac{2R_0}{\left(4 + 6\cos\phi_1(t) - 2\cos^3\phi_1(t)\right)^{\frac{1}{3}}} \tag{39}$$

If we know the contact radius $r_1(t)$ at time t, then we should have $R(t)\sin\phi_1(t) = r_1(t)$. Substituting this into Eq. (39), we have

$$\frac{r_1(t)}{2R_0} = \frac{\sqrt{1 - \cos^2\phi_1(t)}}{\left(4 + 6\cos\phi_1(t) - 2\cos^3\phi_1(t)\right)^{\frac{1}{3}}} \tag{40}$$

Thus, $r_1(t)$ is monotonically decreasing as $\cos\phi_1(t)$ is increasing and we can find an implicit relation as

$$\cos\phi_1(t) = f_1(r_1(t)) \tag{41}$$

Substituting this into Eq. (41), we have

$$R(t) = \frac{2R_0}{\left(4 + 6f_1(r_1(t)) - 2f_1^3(r_1(t))\right)^{\frac{1}{3}}} \triangleq f_2(r_1(t)) \tag{42}$$

then $A^t(t)$ can be written as

$$A^t(t) = A_0 \cdot (1 + S(t)) - \pi f_2^2(r_1(t))(1 - f_1^2(r_1(t))) \triangleq f_3(r_1(t), t) \tag{43}$$

Substituting Eqs. (41)–(43) into the tension–area relation Eq. (37), we have

$$\tau = \frac{\pi^2 K_b}{a_0^2} \exp\left(-\frac{8\pi K_b}{k_B T} \cdot \frac{f_3(r_1(t), t) - 2\pi f_2^2(r_1(t))(1 + f_1(r_1(t)))}{2\pi f_2^2(r_1(t))(1 + f_1(r_1(t)))}\right) \triangleq f_4(r_1(t), t) \tag{44}$$

Also, from Ref. [20], we know the contact radius r_1 propagates toward the Young–Dupre equilibrium Eq. (4) at a rate

$$\dot{r}_1(t) = \frac{\Gamma - (1 - \cos\phi_1(t))\tau}{\eta_0 c_s} \tag{45}$$

where $\eta_0 \approx 10^{-3}\,\text{Pa·s}$ denotes the viscosity of the aqueous medium [28], and c_s denotes surface drag coefficient ranging from hydrodynamic limit ($c_s \approx 1$), through the membrane friction dominated range ($c_s \approx 10^3$), up to surface inhomogeneity governed values ($c_s \approx 10^6$) [20]. In our work, we study the membrane friction dominated range ($c_s \approx 10^3$) used in Ref. [20]. Dragging Eqs. (41) and (44) into Eq. (45), the contact radius rate $\dot{r}_1(t)$ has the form

$$\dot{r}_1(t) = \frac{\Gamma - (1 - f_1(r_1(t)))f_4(r_1(t), t)}{\eta_0 c_s} \tag{46}$$

Although there is no analytic solution for Eq. (46), numerical results can be obtained using a fourth-order Runge–Kutta method. In Fig. 5(*a*) we plot the evolution of contact radius by solving the ordinary differential equation (ODE) Eq. (46) for a vesicle with initial contact radius $r_1^{\text{init}} = 10\,\text{nm}$, initial radius $R_0 = 1.68 \times 10^{-5}$ m and bending modulus $K_b = 21\,k_B T$ under the adhesion energy per unit area $\Gamma = 2.53 \times 10^{-5}$ N/m. Equilibrium is reached at time $t^* = 0.56\,\text{s}$. Our estimate for t^* agrees with a recent theoretical work [20]. Next, we study the effect of Γ on t^*. We choose $\Gamma = 2.53 \times 10^{-4}$ N/m, $\Gamma = 2.53 \times 10^{-5}$ N/m, and $\Gamma = 2.53 \times 10^{-6}$ N/m corresponding to $t^*_{-4}, t^*_{-5}, t^*_{-6}$ (with initial contact radius $r_1^{\text{init}} = 10\,\text{nm}$). The results for the evolution of $r_1(t)$ are shown in Fig. 5(*b*). We can see that $t^*_{-4} \sim 10^{-2}\,\text{s}$, $t^*_{-5} \sim 10^{-1}\,\text{s}$, $t^*_{-6} \sim 10^{0}\,\text{s}$. As expected, increasing Γ increases the speed at which the vesicle finishes its adhesion on the substrate and reaches equilibrium.

3.3 Ordinary Differential Equation Model of Contact Radius Increase With Irradiation. Figure 5(*a*) suggests that t^* is about 0.56 s, which implies that the kinetics of the vesicle adhesion on the substrate is much faster (at least for large enough Γ) than the kinetics of the irradiation, which is hundreds of seconds in Ref. [24] and tens of seconds in Ref. [4]. This shows that the vesicle will completely finish adhesion on the substrate and reach equilibrium as soon as the irradiation is applied. As a consequence, we can separate these two kinetics and only consider the kinetics of irradiation induced oxidation. Here, we consider the three irradiation powers used in Ref. [24]. Let S_1, S_2, S_3 be the surface area increment under irradiation powers 1, 1/4, 1/32, respectively. Then, in order to fit the model in Eqs. (35) and (36), we need to set $k_1 = 0.0427$, 0.0066, 0.0017 and $A_{\text{OX1}} = 1.1936$, 1.1801, 1.1878 under the irradiation power 1, 1/4, 1/32, respectively. The model in Sec. 3.2 can be used here except that we need to replace $S(t) = 0$ by $S_1(t)$, $S_2(t)$, $S_3(t)$. Then, the contact radius $r_1(t)$ at time t can be determined through the Young–Dupre equilibrium Eq. (4)

$$\Gamma = f_4(r_1(t), t) \cdot (1 - f_1(r_1(t))) \tag{47}$$

The results are plotted in Fig. 6(*a*), which shows that higher irradiation power leads to quicker completion of area increase. The k_1 values we found above increase with increasing radiation power, as expected [4]. The curves in Fig. 6(*a*) qualitatively capture the experimental results in Ref. [24] as shown in the inset; a quantitative match may require that we account for the kinetics of OX2. As an alternative, we have used linear interpolation to construct continuous functions for S_1, S_2, S_3 based on discrete data extracted

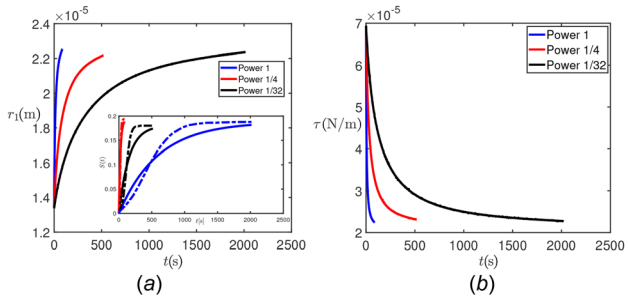

Fig. 6 (*a*) Prediction of time evolution of contact radius r_1 in equilibrium as irradiation is progressing under three different irradiation powers in Ref. [24]. The irradiation power affects the rate constant k_1, which increases as irradiation power increases. The inset is a comparison between fitted functions (solid line) and raw experimental data (dashed line) for surface area increment function $S(t)$ under three different irradiation powers in Ref. [24] showing qualitative agreement. (*b*) Prediction of time evolution of tension τ as irradiation is progressing under three different irradiation powers in Ref. [24]. See online for color version.

from Ref. [24] and performed the exercise above to get better agreement with the experimental data (not shown here). In Fig. 6(*b*), we predict that the tension τ decreases as irradiation progresses. Intuitively, the decrease in tension is expected since the vesicle area increases while its volume is held fixed. Also, experimental evidence [4] shows an increase in thermal fluctuations of the vesicles after irradiation, which is consistent with a reduction in tension. Such a decrease in tension could lead to functional changes in live cells [9]. For example, it has been shown that artificially decreasing membrane tension in fibroblasts increases the rate of cell spreading and lamellipodial extension and stimulates new lamellipodial extensions [29]. Although it has long been known that oxidative damage can cause cell death and diseases [1], changes in cell behavior due to irradiation-induced changes in membrane tension have not been tested in experiments. If such experiments are performed in live cells, then insights from our analysis can inform models for the evolution of cell membrane tension.

4 Kinetics of Detachment of Vesicle After Irradiation

Finally, it is important to study the kinetics of detachment of vesicles from substrates because it represents a stage in cellular processes such as endo- and exo-cytosis, immune response, and cell–tissue interaction [30]. Here, our goal is to determine how irradiation-induced area changes can change the kinetics of detachment.

4.1 Critical Force to Cause Detachment. We consider a detachment process in which the dissociation of bonded ligand–receptor pairs is considered after irradiation has occurred. Following the model in Ref. [17] and Boulbitch [30], we use ρ_1, which is a number per unit area, to denote the local concentration of free ligands in the substrate. Similarly, we use ρ_r to denote the concentration of free receptors in the vesicle wall. Let ρ_{lr} denote the concentration of bonded ligand-receptor pairs. Also, let k_+ be the association rate constant, k_- be the dissociation rate constant. We assume that $\rho_{lr} = \rho_{lr}^{(0)}$ is constant everywhere. Here, $\rho_{\text{lr}}^{(0)}$ is the density of bonded ligand-receptor pairs at equilibrium. Then, the following local rate equation is given by [17]:

$$\frac{d\rho_{\text{lr}}}{dt} = k_+\rho_1\rho_r - k_-\rho_{\text{lr}}^{(0)} \tag{48}$$

where the dissociation rate k_- is given by [31]

$$k_-(f) = k_-^{(0)} \exp\left(\frac{af}{k_BT}\right) \tag{49}$$

where a is the length on the order of 0.1 nm and f is the force on a single bond. We also assume that the vesicle is in equilibrium adhesive contact with the substrate in the absence of detachment force [17]. Then the LHS of Eq. (48) should vanish, and we have

$$k_-^{(0)}\rho_{\text{lr}}^{(0)} = k_+\rho_1\rho_r \tag{50}$$

Substituting this into Eq. (48), we get

$$k_-(f) = \frac{k_+\rho_1\rho_r}{\rho_{lr}^{(0)}} \exp\left(\frac{af}{k_BT}\right) \tag{51}$$

Lin and Freund [17] supposed the applied force on each stretched bond is uniform: $f = F(t)/2\pi r_1(t) b_0 \rho_{lr}^{(0)}$, where $r_1(t)$ is the radius of the adhesion zone at time t and $b_0 \approx 10\,\text{nm}$ is the width of bending zone. Then they show that

$$\frac{dr_1}{dt} = \frac{b_0 k_+\rho_1\rho_r}{\rho_{lr}^{(0)}}\left[1 - \exp\left(\frac{F(t)a}{2\pi b_0 r_1(t)\rho_{lr}^{(0)}k_BT}\right)\right] \tag{52}$$

We first follow the model in Ref. [17] to consider the case when the pulling force is suddenly applied and remains constant during the unbinding process, i.e., $F(t) = F$, $t > 0$. Evans and Ritchie [32] have pointed out that detachment will occur under any level of pulling force if it is held for sufficient time. Therefore, we are interested in the dependence of the dimensionless detachment time τ^* on the constant applied force F with and without irradiation. Let $\beta_1 = Fa/2\pi b_0 k_B T \rho_{lr}^{(0)} R_1$, where R_1 is the initial radius of the adhesion zone under irradiation. Following [17], we use dimensionless variables $\tau_1 = (b_0 k_+\rho_1\rho_r)t/(\rho_{lr}^{(0)}R_1)$, $\xi_1 = r_1/R_1$. Then, Eq. (52) becomes

$$\frac{d\xi_1}{d\tau_1} = 1 - \exp\left(\frac{\beta_1}{\xi_1}\right) \tag{53}$$

with the initial condition $\xi_1(0) = 1$. Similarly, we can define β_2, τ_2, ξ_2 and the ODE with respect to R_2, which is the initial radius of the adhesion zone in the absence of irradiation. It is not hard to see that at a given F, $\beta_1 = C\beta_2$ where C is a constant.

In Boulbitch [30], $k_+\rho_1$ is estimated to be 0.18×10^5/s and in Ref. [17] the receptor density on the substrate surface is about $\rho_r = 1/\mu\text{m}^2$. In Ref. [33], $k_-^{(0)}$ is estimated to be $0.95\,\text{s}^{-1}$. From Fig. 1, in Sec. 2.3, we know $R_1 = 2.38 \times 10^{-5}$ m and $R_2 = 1.34 \times 10^{-5}$ m. Then, β_1 and β_2 should be in the range $4.30 \times 10^{-9} < \beta_1 < 4.30 \times 10^{-6}$ and $7.64 \times 10^{-9} < \beta_2 < 7.64 \times 10^{-6}$, respectively, which corresponds to $0.5\,\text{pN} < F < 500\,\text{pN}$ used by Lin and Freund [17]. In particular, for a given F, $\beta_2/\beta_1 \approx 1.78$. We numerically integrate Eq. (52) using these numbers and plot the result in Fig. 7(*a*) in which $\beta = \beta_1$ is a "reference dimensionless variable." Within the force range mentioned above, the dependence of the dimensionless detachment time τ_1^*, τ_2^* (corresponding to dimensionless detachment time with and without irradiation), respectively, on β_1, β_2 is

$$\tau_1^* \propto \beta_1^{-1.00}, \quad \tau_2^* \propto \beta_2^{-1.00} \tag{54}$$

Since β_1 and β_2 are proportional to F, we have

$$\tau^* \propto F^{-1.00}, \quad (F \text{ between } 0.5\,\text{pN and } 500\,\text{pN}) \tag{55}$$

Note that Eq. (55) holds for both cases (with and without irradiation). The time to detachment will be higher after irradiation because a larger area is adhered.

Now, we consider a time-dependent force at constant rate $\dot{F}$ as proposed by Lin and Freund [17]. Let $F(t) = \dot{F}t$, then Eq. (55) can be rewritten as

$$\frac{d\xi}{d\tau} = 1 - \exp\left(\eta\frac{\tau}{\xi}\right) \tag{56}$$

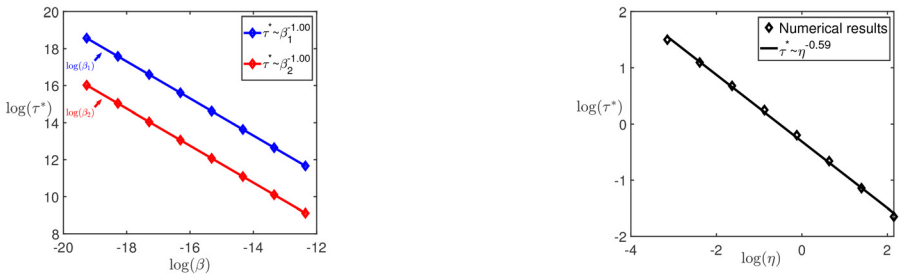

(*a*) (*b*)

Fig. 7 (*a*) Prediction of dependence of dimensionless detachment time τ^* on β_1 and β_2 under the same constant force *F*. (*b*) Prediction of dependence of dimensionless detachment time τ^* on η which implies the dependence of real detachment time μ^* on loading rate $\dot{F}$.

where $\eta = \dot{F}a/(2\pi b_0^2 k_+ \rho_1 \rho_r k_B T)$. Using the values of these parameters mentioned above, we have $\eta = 2.15 \times 10^9 \dot{F}$. As pointed out by Prechtel et al. [25], the force rate $\dot{F}$ in experiments is estimated to be between 20 pN/s and 4 nN/s, which corresponds to η between 0.043 and 8.6. Equation (56) can be integrated numerically and the result is plotted in Fig. 7(*b*) as symbols. The fitted line reveals that $\tau^* \approx \eta^{-0.59}$. Let the real detachment time be μ^*. We want to study the dependence of the dimensionless detachment time τ^* on η and, accordingly, the dependence of the real detachment time μ^* on the force rate $\dot{F}$ with and without irradiation. Recall that μ^* is proportional to τ^* and $\dot{F}$ is proportional to η. It follows from Fig. 7(*b*) that within the range $0.043 < \eta < 8.6$, the dependence of the real detachment time μ^* on the force rate $\dot{F}$ can be approximated by a power law as $\mu^* \propto (\dot{F})^{-0.59}$. Since the detachment force $F^* = \dot{F}\mu^*$, this implies

$$F^* \propto (\dot{F})^{0.41} \tag{57}$$

We note that Fig. 7(*b*) and Eq. (57) works for both cases (with and without irradiation). The only difference comes from the real detachment time μ^*. If we use μ_1^* to denote the detachment time under irradiation and μ_2^* without irradiation, then we should have, as expected, $\mu_1^*/\mu_2^* = R_1/R_2 = 1.78$.

5 Conclusion

In this paper, we investigated the mechanics of a vesicle subject to adhesion, micropipette aspiration, and irradiation simultaneously. We computed the shapes of the vesicles at equilibrium and also studied the kinetics of competing processes such as adhesion and irradiation-induced oxidation. An important aspect of our computations is that thermal undulations of the lipid membrane are taken into consideration so that they can be realistically compared to adhesion and irradiation experiments. The time variation of the mechanical moduli of irradiated vesicles is also taken into account in our computations. As such, our results are in agreement with several experimental papers on oxidation induced structural changes in vesicles. For example, we predicted the kinetics of the area increment of a lipid membrane sucked into a micropipette under different irradiation powers and the dynamics of the contact radius during adhesion, which are in agreement with experiments. We have also made falsifiable predictions that can be tested in future experiments. Our model may be extended to account for pore formation in oxidized membranes, but we leave this to the future.

Funding Data

- United States National Science Foundation (CMMI 1662101, Funder ID. 10.13039/100000001).

References

[1] Pap, E., Drummen, G., Winter, V., Kooij, T., Rijken, P., Wirtz, K., Op den Kamp, J., Hage, W., and Post, J., 1999, "Ratio-Fluorescence Microscopy of Lipid Oxidation in Living Cells Using c11-Bodipy581/591," FEBS Lett., **453**(3), pp. 278–282.

[2] Droge, W., 2002, "Free Radicals in the Physiological Control of Cell Function," Physiol. Rev., **82**(1), pp. 47–95.

[3] Haluska, C. K., Baptista, M. S., Fernandes, A. U., Schroder, A. P., Marques, C. M., and Itri, R., 2012, "Photo-Activated Phase Separation in Giant Vesicles Made From Different Lipid Mixtures," Biochim. Biophys. Acta, **1818**(3), pp. 666–672.

[4] Sankhagowit, S., Wu, S.-H., Biswas, R., Riche, C. T., Povinelli, M. L., and Malmstadt, N., 2014, "The Dynamics of Giant Unilamellar Vesicle Oxidation Probed by Morphological Transitions," Biochim. Biophys. Acta, **1838**(10), pp. 2615–2624.

[5] Aoki, P. H., Morato, L. F., Pavinatto, F. J., Nobre, T. M., Constantino, C. J., and Oliveira, O. N., Jr., 2016, "Molecular-Level Modifications Induced by Photo-Oxidation of Lipid Monolayers Interacting With Erythrosin," Langmuir, **32**(15), pp. 3766–3773.

[6] Barrow, D. A., and Lentz, B. R., 1981, "A Model for the Effect of Lipid Oxidation on Diphenylhexatriene Fluorescence in Phospholipid Vesicles," Biochim. Biophys. Acta, **645**(1), pp. 17–23.

[7] Weber, G., Charitat, T., Baptista, M. S., Uchoa, A. F., Pavani, C., Junqueira, H. C., Guo, Y., Baulin, V. A., Itri, R., Marques, C. M., and Schroder, A. P., 2014, "Lipid Oxidation Induces Structural Changes in Biomimetic Membranes," Soft Matter, **10**(24), pp. 4241–4247.

[8] Benet, E., and Vernerey, F. J., 2016, "Mechanics and Stability of Vesicles and Droplets in Confined Spaces," Phys. Rev. E, **94**(6–1), p. 062613.

[9] Diz-Muñoz, A., Fletcher, D. A., and Weiner, O. D., 2013, "Use the Force: Membrane Tension as an Organizer of Cell Shape and Motility," Trends Cell Biol., **23**(2), pp. 47–53.

[10] Purohit, P. K., and Smith, D. H., 2016, "A Model for Stretch Growth of Neurons," J. Biomech., **49**(16), pp. 3934–3942.

[11] Liu, L., and Sharma, P., 2013, "Flexoelectricity and Thermal Fluctuations of Lipid Bilayer Membranes: Renormalization of Flexoelectric, Dielectric, and Elastic Properties," Phys. Rev. E, **87**(3), p. 032715.

[12] Walani, N., Torres, J., and Agrawal, A., 2015, "Endocytic Proteins Drive Vesicle Growth Via Instability in High Membrane Tension Environment," Proc. Natl. Acad. Sci. U.S.A., **112**(12), pp. E1423–E1432.

[13] Brochard-Wyart, F., and de Gennes, P.-G., 2009, "Unbinding of Adhesive Vesicles," *PG De Gennes' Impact on Science-Volume II: Soft Matter and Biophysics*, World Scientific, Singapore, pp. 139–145.

[14] Veerapaneni, S. K., Gueyffier, D., Biros, G., and Zorin, D., 2009, "A Numerical Method for Simulating the Dynamics of 3D Axisymmetric Vesicles Suspended in Viscous Flows," J. Comput. Phys., **228**(19), pp. 7233–7249.

[15] Perez, S., Sergent, O., Morel, P., Chevanne, M., Dubos, M., Cillard, P., and Cillard, J., 1995, "Kinetics of Lipid Peroxidation Induced by UV Beta Rays in Human Keratinocyte and Fibroblast Cultures," C. R. Seances. Soc. Biol. Ses. Fil., **189**(3), pp. 453–465.

[16] Seifert, U., 1997, "Configurations of Fluid Membranes and Vesicles," Adv. Phys., **46**(1), pp. 13–137.

[17] Lin, Y., and Freund, L., 2007, "Forced Detachment of a Vesicle in Adhesive Contact With a Substrate," Int. J. Solids Struct., **44**(6), pp. 1927–1938.

[18] Rim, J. E., Purohit, P. K., and Klug, W. S., 2014, "Mechanical Collapse of Confined Fluid Membrane Vesicles," Mech. Model. Mechanobiol., **13**(6), pp. 1277–1288.

[19] Boal, D., and Boal, D. H., 2012, *Mechanics of the Cell*, Cambridge University Press, Cambridge, UK.

[20] Takáts-Nyeste, A., and Derényi, I., 2014, "Rupture of Lipid Vesicles Near Solid Surfaces," Phys. Rev. E, **90**(5), p. 052710.

[21] Hategan, A., Law, R., Kahn, S., and Discher, D. E., 2003, "Adhesively-Tensed Cell Membranes: Lysis Kinetics and Atomic Force Microscopy Probing," Biophys. J., **85**(4), pp. 2746–2759.
[22] Evans, E., and Rawicz, W., 1990, "Entropy-Driven Tension and Bending Elasticity in Condensed-Fluid Membranes," Phys. Rev. Lett., **64**(17), pp. 2094–2097.
[23] Kühnel, W., 2013, "Differential Geometry," Am. Math. Soc., **77**, pp. 80–81.
[24] Aoki, P., Schroder, A., Constantino, C., and Marques, C., 2015, "Bioadhesive Giant Vesicles for Monitoring Hydroperoxidation in Lipid Membranes," Soft Matter, **11**(30), pp. 5995–5998.
[25] Prechtel, K., Bausch, A., Marchi-Artzner, V., Kantlehner, M., Kessler, H., and Merkel, R., 2002, "Dynamic Force Spectroscopy to Probe Adhesion Strength of Living Cells," Phys. Rev. Lett., **89**(2), p. 028101.
[26] Olbrich, K., Rawicz, W., Needham, D., and Evans, E., 2000, "Water Permeability and Mechanical Strength of Polyunsaturated Lipid Bilayers," Biophys. J., **79**(1), pp. 321–327.
[27] Kučerka, N., Tristram-Nagle, S., and Nagle, J. F., 2006, "Structure of Fully Hydrated Fluid Phase Lipid Bilayers With Monounsaturated Chains," J. Membr. Biol., **208**(3), pp. 193–202.
[28] Arroyo, M., and DeSimone, A., 2009, "Relaxation Dynamics of Fluid Membranes," Phys. Rev. E, **79**(3), p. 031915.
[29] Hood, J. D., and Cheresh, D. A., 2002, "Role of Integrins in Cell Invasion and Migration," Nat. Rev. Cancer, **2**(2), pp. 91–100.
[30] Boulbitch, A., 2003, "Enforced Unbinding of Biomembranes Whose Mutual Adhesion is Mediated by a Specific Interaction," Eur. Biophys. J., **31**(8), pp. 637–642.
[31] Bell, G. I., 1978, "Models for the Specific Adhesion of Cells to Cells," Science, **200**(4342), pp. 618–627.
[32] Evans, E., and Ritchie, K., 1997, "Dynamic Strength of Molecular Adhesion Bonds," Biophys. J., **72**(4), pp. 1541–1555.
[33] Alon, R., Hammer, D. A., and Springer, T. A., 1995, "Lifetime of the p-Selectin-Carbohydrate Bond and Its Response to Tensile Force in Hydrodynamic Flow," Nature, **374**(6522), pp. 539–542.